**ARTICLE**     OPEN

Check for updates

# Unleashing the power of the Sun: the increasing impact of the solar cycle on off-season super typhoons since the 1990s

Chau-Ron Wu[1 ✉], Yong-Fu Lin[2], I-I Lin [ID][3] and Jin-Yi Yu [ID][2 ✉]

The occurrence of super typhoons outside the normal typhoon season can result in devastating loss of life and property damage. Our research reveals that the 11-year solar cycle can affect the incidence of these off-season typhoons (from November to April) in the western North Pacific by influencing sea surface temperature (SST) through a footprint mechanism. The solar cycle, once amplified by atmospheric and ocean interactions, generates a noticeable SST footprint in the subtropical North Pacific during winter and spring, which eventually intrudes into the tropical central Pacific and affects the atmospheric conditions, resulting in an increase or decrease in the occurrence of super typhoons during active or inactive solar periods. This mechanism has become more effective since the Atlantic Multi-decadal Oscillation (AMO) shifted to a warm phase in the 1990s, intensifying the subtropical Pacific couplings. An example of this type of off-season super typhoon during an active solar period is Typhoon Haiyan in 2013. By incorporating information about the solar cycle, we can anticipate the likelihood of super typhoon occurrences, thus improving decadal disaster preparation and planning.

## INTRODUCTION

In the western North Pacific, typhoons typically occur from May to October, when atmospheric and oceanic conditions such as wind shear and sea surface temperatures (SSTs) are favorable for typhoon formation. However, in rare instances, typhoons can still develop during the off-season (November–April), when these conditions are generally unfavorable, if other factors align to create the necessary conditions for typhoon formation. The occurrence of super typhoons (categories 4 and 5 on the Saffir–Simpson scale) during this off-season can result in extensive damage to property and loss of life. For instance, Typhoon Haiyan, which was a category 5 typhoon with maximum wind speeds of over 170 knots, made landfall in the Philippines on November 8, 2013, causing catastrophic destruction due to strong storm surges, extremely high winds, and intense rainfall[1,2].

According to the best track database from the US Joint Typhoon Warning Center, a total of 402 off-season typhoons occurred in the western North Pacific between 1945 and 2018. These typhoons had a season-mean genesis position within the off-season main development region (OMDR)[3] of 4–15°N and 122–180°E (as shown in Fig. 1a). The number of off-season super typhoons varies each year, with a maximum of four events in 1955 and 1990 and no events in some years (as shown in Fig. 1b). Interestingly, the number of off-season super typhoons appears to be correlated with the yearly sunspot number (SSN), especially in recent decades. The sunspot number serves as a proxy for solar activity during the well-known 11-year solar cycle[4,5], which can affect the total solar irradiance (TSI) reaching the Earth's surface. The SSN time series shows maxima and minima, representing active and inactive periods of the solar cycle, respectively, and associated with relatively large and small TSIs (as shown in Supplementary Fig. 1).

As shown in Fig. 1b, the SSN time series fluctuates at an 11-year frequency and the co-variation between the SSN and off-season super typhoon number indicates that more super typhoons occur

during active solar cycle periods compared to inactive periods. No such correlation exists between SSN and the total off-season typhoon numbers (i.e., including both super and regular typhoons) (see Supplementary Fig. 2), indicating that the solar cycle may have a particularly strong influence on the occurrence of super typhoons. A lead-lag correlation analysis (as shown in Supplementary Fig. 3) reveals that the strongest correlation between these two time series occurs when the SSN leads the super typhoon number by 1 year. As will be described in detail later, the solar cycle-induced sea surface temperature footprint typically appears first in winter and develops into the spring of the following year to impact off-season typhoons, thus there is a 1-year lag between the yearly SSN time series and that of off-season super typhoons. A 21-year running correlation analysis (as shown in Fig. 1c) further shows that the modulating effect increased during the 1990s and has remained high since. Two questions need to be answered: (1) what is the physical mechanism enabling the 11-year solar cycle to modulate the occurrence of off-season super typhoons and (2) why did the modulating effect intensify after the 1990s?

## RESULTS

### Solar cycle impacts on the atmospheric or oceanic environments for typhoons

We concentrate on the most prominent period of modulation, 1985–2018 (the period highlighted in yellow in Fig. 1b), to uncover the underlying mechanism. During this time frame, there were a total of 206 off-season typhoons and the correlation between the yearly sunspot number (SSN) and the number of off-season super typhoons was statistically significant ($R = 0.60$, $P < 0.1$) with a 1-year lag. For example, Typhoon Haiyan in 2013 took place during the peak of the latest active period of the solar cycle. The power spectrum of the yearly number of off-season super typhoons during this period displays a clear and significant peak

[1]Department of Earth Sciences, National Taiwan Normal University, Taipei, Taiwan. [2]Department of Earth System Science, University of California, Irvine, CA, USA. [3]Department of Atmospheric Sciences, National Taiwan University, Taipei, Taiwan. ✉email: cwu@ntnu.edu.tw; jyyu@uci.edu

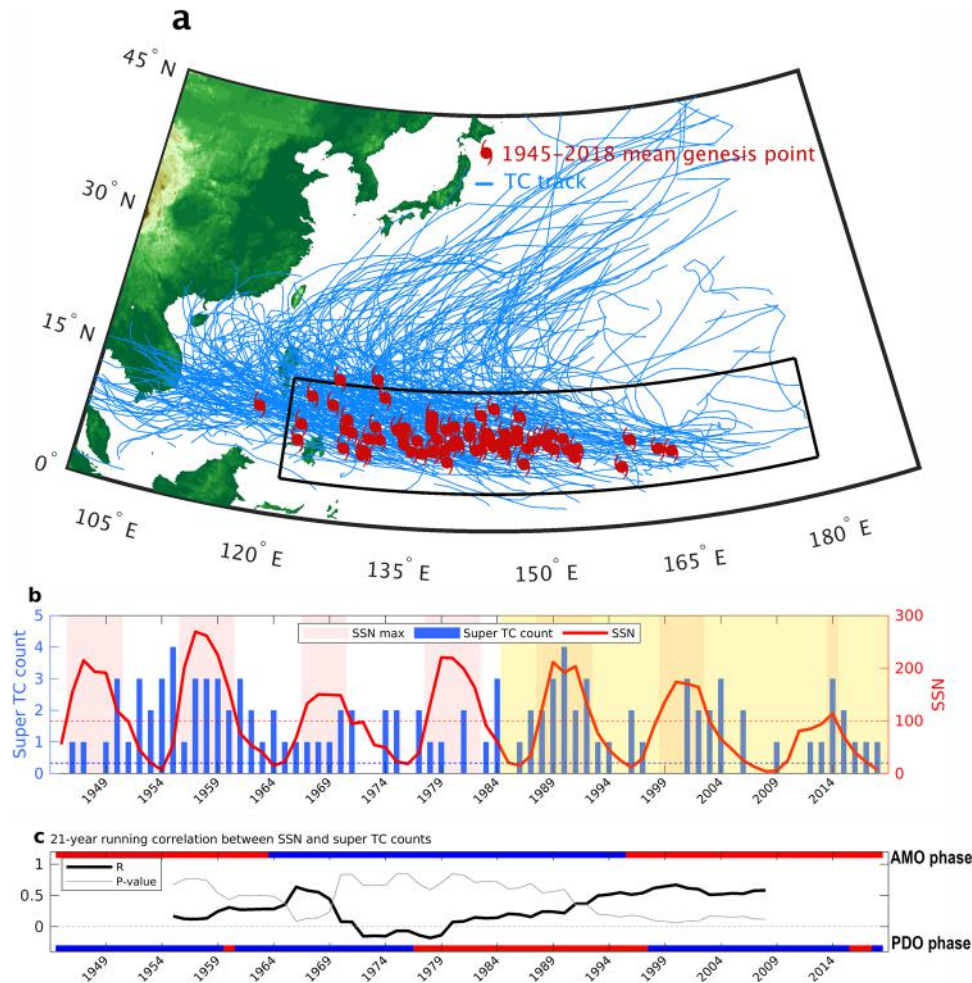**Fig. 1 Annual occurrence of off-season super typhoons and its correlation with solar sunspot number (SSN). a** The blue lines represent the trajectories of the 402 off-season typhoons (with maximum wind speeds ≥34 knots) during the period 1945–2018, and the red dots show their annual mean genesis positions. The black box denotes the main development region (OMDR) for these typhoons. **b** The time series plot displays the yearly (January–December) SSN numbers (red line) and the number of off-season super typhoons (categories 4 and 5; blue bars) in the western North Pacific during the period 1945–2018. The red and blue-dashed lines denote the thresholds used to define $SSN_{max}$ ($SSN \geq 100$, active) and $SSN_{min}$ ($SSN \leq 20$; inactive) periods of the solar cycle, respectively. The active periods are shaded pink. **c** The 21-year running correlation between the yearly SSN and the number of off-season super typhoons at a 1-year lag (i.e., SSN leading the typhoon number by 1 year) is displayed using the black line for the correlation coefficient and gray line for the $P$ value. The red and blue shadings at the top and bottom of (**c**), respectively, indicate the positive and negative phases of the Atlantic Multi-decadal Oscillation (AMO) and Pacific Decadal Oscillation (PDO) determined using index values obtained by applying a 7-year running mean.

near the 11-year band (Supplementary Fig. 4). To ascertain that the correlation truly arises from the 11-year solar cycle rather than being attributed to alternative climate variability modes like ENSO, Pacific Decadal Oscillation (PDO), and Atlantic Multi-decadal Oscillation (AMO), a further investigation was undertaken. We conducted an additional round of 1-year lag correlations after meticulously eliminating the influences of these climate modes from the off-season typhoon number time series. The influence of ENSO was first removed through the application of a 7-year running mean. Following this, the impacts of PDO and AMO were distinctly eradicated using linear regression methods. As depicted in Supplementary Table 1, the resulting correlations exhibited a high degree of consistency with those attained prior to the removal of these climate-related signals. This outcome strongly indicates that the relationship between the 11-year cycle and the super typhoon count remains robust, and it remains unperturbed by these internal modes of climate variability.

The solar cycle must impact the large-scale atmospheric or oceanic environments, or both, in which typhoons form, in order to modulation in their occurrence. Oceanic conditions, such as

$SST$[6] and upper-ocean heat content (UOHC)[7–10], can influence typhoon activity. UOHC, also referred to as tropical cyclone heat potential, is the amount of heat contained between the sea surface and the depth of the 26 °C isotherm (D26) and is used to quantify the thickness of the warm subsurface ocean layer[8]. During the period of 1985–2018, the strongest modulation period as indicated in Fig. 1b, the off-season (November–April) SST and D26 in the main development region (OMDR) showed a negative regression with the yearly SSN (Supplementary Figs. 5a and 6). This means that during active solar periods, the OMDR tends to have colder SSTs and a shallower warm ocean layer, which are unfavorable conditions for typhoon development. As a result, these oceanic conditions cannot explain why more off-season super typhoons occur during active periods of the solar cycle.

Atmospheric conditions, such as vertical wind shear (VWS) and low-level relative vorticity (at 850 hPa), play a critical role in typhoon development. The dynamic genesis potential index (DGPI) is often used as a broader measure of atmospheric conditions, considering not only these two key variables but also the vertical velocity (at 500 hPa) and the meridional gradient of
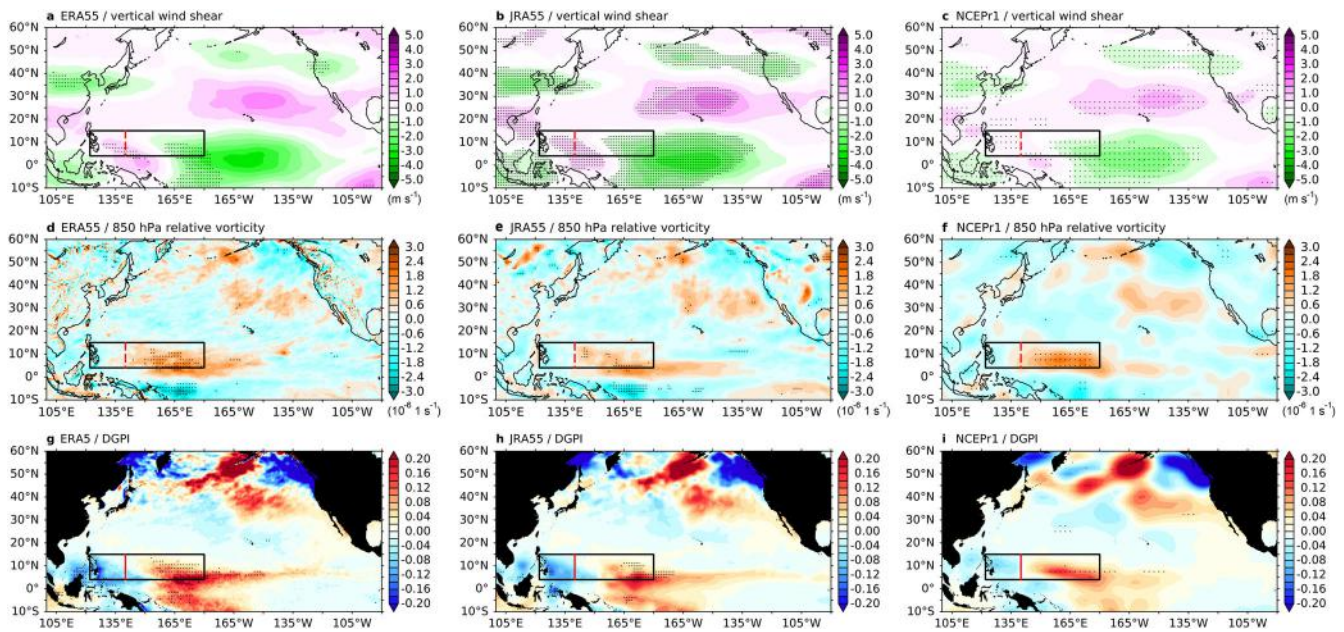
**Fig. 2 Atmospheric responses to the solar cycle in the North Pacific during typhoon off-season (November to April).** The colors in (**a**–**c**) represent the regressions of vertical wind shear (unit in m s$^{-1}$) for off-season (November–April) for ERA5, JRA55, and NCEPr1, respectively. **d**–**f** are similar to (**a**–**c**), respectively, but for 850-hPa relative vorticity (unit in $10^{-6}$ 1 s$^{-1}$), with the regressions being made onto the yearly normalized sunspot number (SSN) at a 1-year lag, meaning SSN leads by 1 year. The period of analysis is from 1985–2018. **g**–**i** is similar to (**a**–**c**), but for dynamic genesis potential index (DGPI). The stippled areas in the figures indicate regions where the regressions are significant at a 90% confidence level as determined by a Student's $t$ test. The black boxes denote the main development region of the off-season typhoons (OMDR).

zonal wind (at 500 hPa) for typhoon genesis[11] (see Materials and Methods). We examine in Fig. 2 the 1-year lagged regressions of off-season VWS, relative vorticity at 850 hPa, and DGPI against the yearly SSN, using data from 1985–2018. To reinforce the reliability of the results, the analysis was performed using three reanalysis products: NCEPr1, ERA5, and JRA55. The results indicate that in the OMDR, particularly to the east of 140°E, the regressions are negative for VWS, positive for relative vorticity, and positive for DGPI. The weaker VWS, higher relative vorticity, and higher DGPI indicate a favorable atmospheric environment for typhoon development[12–16] during the active periods of the 11-year solar cycle. Given the positive correlation between off-season typhoon occurrence and SSN number (as seen in Fig. 1b), the favorable atmospheric conditions must overpower the unfavorable oceanic conditions in modulating the number of off-season super typhoons during the solar cycle. The analyses were repeated using data from 1948–2018, resulting in similar but weaker results (Supplementary Figs. 5b and 7). The similarity confirms the robustness of the modulation mechanism identified in the shorter 1985–2018 period throughout the entire analysis period. The robustness of the results is further evaluated through coupled climate model experiments in a later section of this study. It is important to note that the analyses of D26 were not repeated due to the shortage of datasets of sufficient length.

We next examine the impact of solar cycle-induced atmospheric conditions on the genesis, propagation, and intensity of off-season typhoons during 1985–2018 (Fig. 3a). The average genesis position of typhoons during SSN$_{max}$ periods (high solar activity, indicated by the red dot located at approximately 10°N and 144°E) is located approximately 5° southeast of the average genesis position during SSN$_{min}$ periods (low solar activity, indicated by the blue dot located at around 11°N and 139°E) (Fig. 3a, b). This suggests that off-season typhoons tend to form farther from land during active solar periods compared to inactive periods. This aligns with the favorable atmospheric conditions for typhoon

development, which are present in the east of 140°E within the OMDR during active periods (see Fig. 2).

Figure 3a also shows that typhoons during active solar periods tend to turn northward more frequently than those during inactive periods, which tend to propagate more directly westward. As a result, active-period typhoons remain over the ocean longer, due to their more eastward genesis locations and northward-turning trajectories. This results in a longer mean typhoon duration of 135.7 hours during active periods ($P < 0.01$, Fig. 3c), which is 1.3 times the mean duration during inactive periods (103.7 h, $P < 0.01$, Fig. 3c). This longer duration allows the typhoons to absorb more energy from the ocean, enhancing their intensity[3,17,18] and increasing the frequency of super typhoons during active solar periods. To quantify typhoon strength, we use the lifetime maximum intensity (LMI) and power dissipation index (PDI), which LMI is defined using maximum surface wind speed over the lifetime of a tropical cyclone[19–21] and PDI is calculated as the sum of the 6-hourly maximum surface wind speeds in a cubic volume over the lifetime of a tropical cyclone[22]. As shown in Fig. 3d, e, the average LMI for typhoons during active solar periods is 1.3 times that of those during inactive solar periods, whereas the average PDI for typhoons during active solar periods is 1.4 times that of those during inactive periods. The impact of the solar cycle on the intensity of off-season typhoons is further supported by the positive correlation coefficient ($R = 0.55$, $P < 0.1$, SSN leads by 1 year) between the yearly SSN and the season-mean PDI during the analysis period (Fig. 3e).

## The mechanism linking the solar cycle to typhoon environments

We next aim to understand the mechanism that allows the 11-year solar cycle to affect atmospheric conditions in the tropical Pacific during the typhoon off-season. In addition to the surface cooling in the OMDR, we observe that SST differences between the active and inactive periods of the solar cycle also present themselves as a
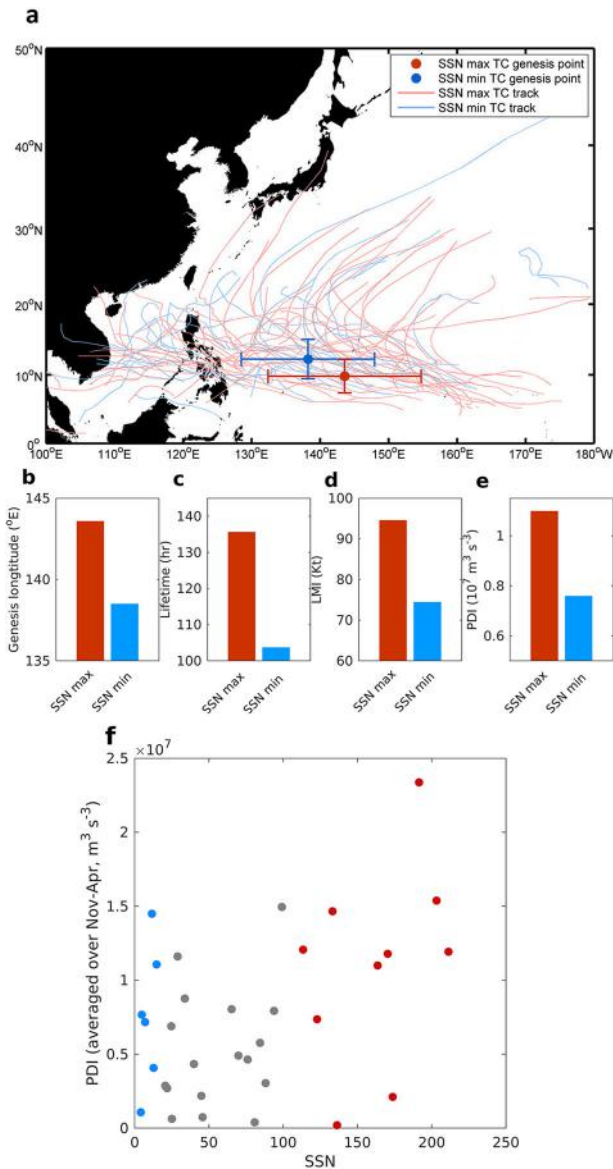
**Fig. 3 Impacts of the 11-year solar cycle on typhoon genesis, trajectory, lifetime maximum intensity (LMI), and the power dissipation index (PDI). a** The average typhoon genesis positions are shown as dots with the one standard deviation range indicated by bars. The positions are represented in red ($SSN_{max}$ or active period) and blue ($SSN_{min}$ or inactive period) during the period 1985–2018. The thin red and blue lines represent the typhoon trajectories during the $SSN_{max}$ and $SSN_{min}$ periods, respectively. **b** The mean genesis longitude, **c** the typhoon duration, **d** the LMI, and **e** the PDI are displayed as average values for off-season typhoons during $SSN_{max}$ and $SSN_{min}$ periods, represented in red and blue bars, respectively. All differences between $SSN_{max}$ and $SSN_{min}$ in (**b**–**e**) are significant at the 99% confidence level as determined by a Student's t test. **f** A scatter diagram is shown to demonstrate the relationship between SSN and PDI during the analysis period.

meridional pattern of surface warming that spreads from the northeastern Pacific to the tropical central Pacific (Supplementary Fig. 5). This pattern has been recognized by recent studies[23,24] as the SST footprint of the 11-year solar cycle in the Pacific. They postulate that the radiative forcing associated with the solar cycle is first intensified in the stratosphere through its interaction with the Brewer–Dobson circulation (BDC)[3,25]. During active periods of the cycle, the weakened BDC leads to anomalous descending

motion in the tropics that extends into the upper troposphere, reducing the rising branch of the Hadley circulation. This weakening of the Hadley circulation causes a decrease in subsidence over the northeastern Pacific and weakens the Pacific High, resulting in weaker trade winds, reduced surface evaporation, and warmer SSTs over the northeastern Pacific. The warmer SSTs can spread toward the tropical central Pacific through subtropical Pacific atmosphere-ocean coupling processes[26,27], eventually creating the meridional pattern of SST warming in Supplementary Fig. 5. Conversely, during inactive periods, a cold SST footprint is observed. Previous research has demonstrated that subtropical coupling processes are most efficient during the boreal winter and spring[28], and that the SST footprint typically reaches the tropical Pacific by boreal spring the following year[29]. This seasonality of the subtropical Pacific coupling processes is why the strongest correlation between the yearly SSN and the yearly number of off-season super typhoons occurs when the former leads the latter by 1 year (Supplementary Fig. 2).

The mechanism by which the 11-year solar cycle modulates atmospheric conditions in the tropical Pacific during boreal winter and spring (typhoon off-season) suggested by Lin et al.[23] can be confirmed for the period 1985–2018 using the three reanalysis products employed in this study (Fig. 4). Figure 4a, c, e depict the regression of the off-season streamfunction over the Northeastern Pacific (NEP, 150°W-100°W) onto the yearly normalized observed SSN. The negative values between 0 and 30°N indicate a weakening (strengthening) of the Hadley circulation during active (inactive) periods of the solar cycle. Similar regressions with sea level pressure and 850-hPa wind (Fig. 4b, d, f) support the conclusion that the subtropical Pacific high and northeasterly trade winds are weakened (strengthened) during active (inactive) periods. During the active periods, the weakening of the subtropical high results in reduced trade winds on its southeastern flank, which leads to warm SST anomalies. These anomalies then spread from the northeastern Pacific to the tropical central Pacific (as seen in Supplementary Fig. 5). The solar SST footprint intrudes into the tropics, causing warmer SSTs in the tropical central-to-eastern Pacific and leading to a weakening of the mean Pacific Walker circulation during active periods (as evidenced by the anomalous westerlies over the tropical western-to-central Pacific in Fig. 4b, d, f). This weakening, combined with the warmer SSTs in the tropical central Pacific, shifts convection eastward, causing a decrease in VWS and an increase in low-level relative vorticity. These effects explain why off-season typhoons have a more eastward mean genesis position during active periods compared to inactive periods (as shown in Fig. 3a, b). Additionally, the reduced mean trade winds during active periods slow the lateral movement of typhoons, enabling them to spend more time over the tropical Pacific and develop into super typhoons (as demonstrated in Fig. 3c, d). The results are consistent when the analysis is repeated using data from the entire 1948–2018 period (as seen in Supplementary Fig. 8). These analyses demonstrate that the 11-year solar cycle, through its SST footprint mechanism, can create favorable (unfavorable) atmospheric conditions during its active (inactive) periods, resulting in an increase (decrease) in the occurrence of off-season super typhoons.

To further verify the impact mechanism of the solar cycle, we conducted both idealized and realistic sets of solar forcing experiments using coupled climate models (see the "Methods" section for a detailed description of the experiments). In the idealized experiments, we included or excluded an artificially-enhanced solar forcing in the CESM1 model to investigate the impact of the solar cycle on the large-scale atmospheric and oceanic conditions that are critical for typhoon development. In the control experiment, the TSI was maintained constant. Conversely, in the solar experiment, it was varied according to the five-times amplified amplitude of the observed solar cycle
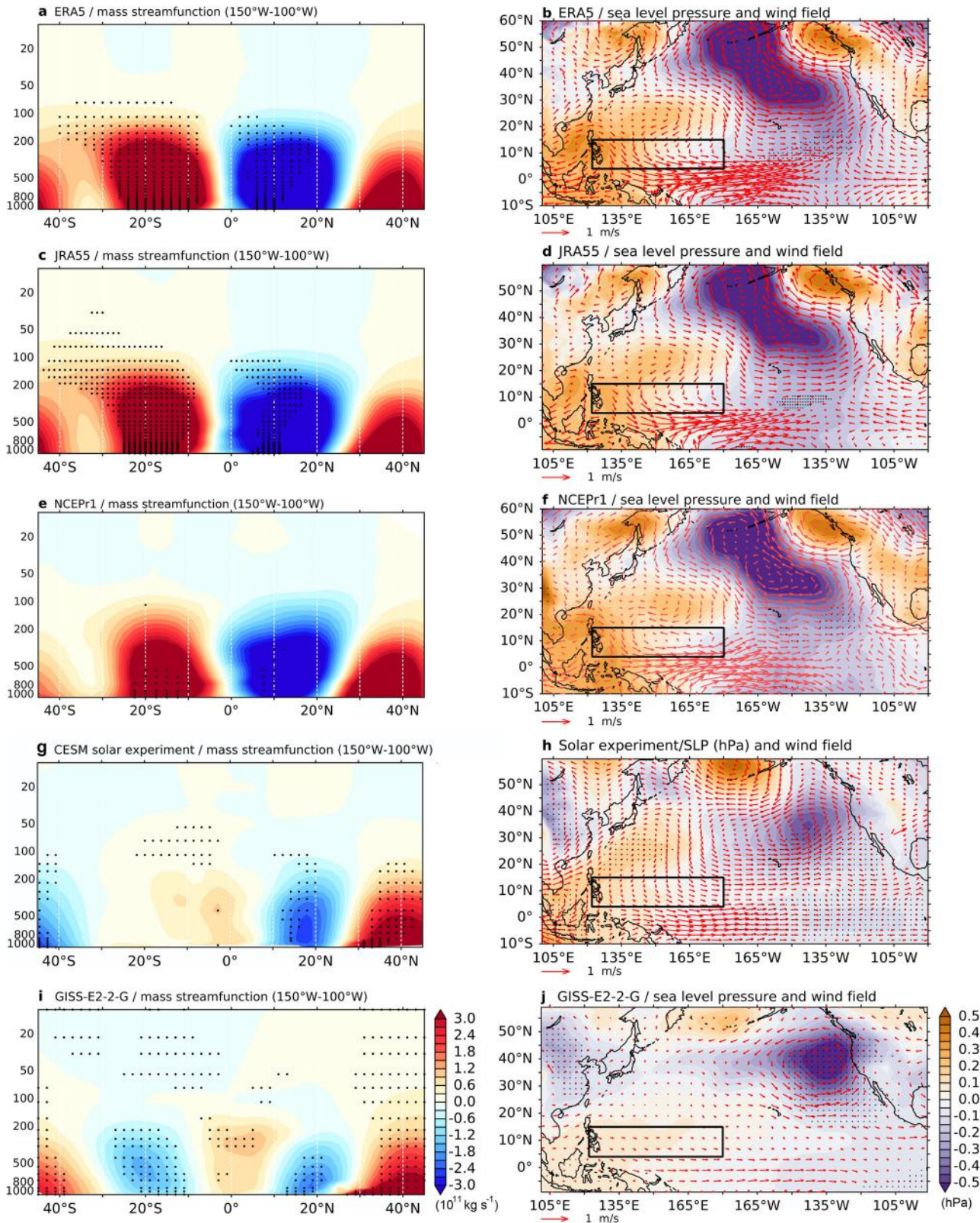
**Fig. 4 Atmospheric circulation responses to solar forcing.** Regressions of the off-season (November to April) for **a** ERA5 Northeastern Pacific (NEP, 150°W–100°W) mass streamfunction (colors, unit is $10^{11}$ kg s$^{-1}$) and **b** sea level pressure (colors, unit is hPa) and 850-hPa wind (arrows, unit is m s$^{-1}$) onto the yearly normalized SSN at a 1-year lag (i.e., SSN leads by 1 year) during the period 1985–2018 are shown. **c–f** present the same information as (a, **b**), but for the JRA55 and NCEPr1 data, respectively. **g, h** present the same information as (a, **b**), but for the CESM1 solar experiment and the regressions onto the yearly normalized Total Solar Irradiance (shown in Fig. S9a). **i, j** present the same information as (a, **b**), but for the regressions onto the yearly normalized Total Solar Irradiance (shown in Fig. S9b) in the CMIP6 GISS-E2-2-G historical-solar experiment. The black boxes in (**b**, **d**, **f**, **h**, **j**) indicate the OMDR. The stippled areas indicate where the regressions are significant at the 90% confidence level, as determined by a Student's $t$ test.

variations during AD850–959, as indicated by the red line in Supplementary Fig. 9a. This amplification was carried out to more noticeably display the impact of the solar cycle, eliminating the need to account for the realistic simulation of the stratospheric amplification of the solar cycle forcing by the CESM1 model. Both the control and solar experiments were run for 110 years (AD850–959) using pre-industrial forcing to exclude any anthropogenic influence. In the realistic solar forcing experiment, the observed solar cycle forcing during the historical period (1850–2014; Supplementary Fig. 9b) was included in a 165-year simulation produced by the high-top version of the GISS-E2-2-G model (referred to as the GISS-E2-2-G hist-sol simulation). All other external forcing factors, such as greenhouse gas concentrations and aerosol amounts, were fixed at pre-industrial levels. This experiment was designed to test the impacts of the solar cycle forcing after it was amplified by the reasonably simulated stratospheric amplification mechanism in the high-top model. Hence, this experiment serves as a check for the impacts of the solar cycle forcing.

We first examine the power spectra of the Pacific Meridional Mode (PMM) index in the CESM1 experiments and the GISS-E2-2-G hist-sol simulation (Supplementary Fig. 10). The PMM index is used to quantify the SST variations over the region where the solar SST footprint is observed. We find that a significant spectral peak near the 11-year band appears in the CESM1 solar-forced experiment and the GISS-E2-2-G hist-sol simulation, but it is not present in the CESM1 control experiment. The regression of SSTs from the CESM1 solar-forced experiment and the GISS-E2-2-G hist-sol simulation onto the yearly TSI prescribed in those experiments (Supplementary Fig. 11) shows a region of warm SST anomalies extending from the northeastern Pacific to the tropical central Pacific, which resembles the solar SST footprint seen in the observational analysis (see Supplementary Figs. 11 and 5). The 1-year lag correlation between the PMM index and TSI also increases from the control run ($R = 0.08$; $P > 0.1$) to the solar forcing experiment ($R = 0.57$; $P < 0.01$) conducted with the CESM1, confirming the impact of the 11-year solar cycle on the PMM pattern of SST anomalies.

The regression of the zonal-mean atmospheric temperatures in these two solar-forced experiments onto the prescribed TSI confirms that solar forcing warms the lower stratosphere and upper troposphere (Supplementary Fig. 12). This warming reduces atmospheric instability during the active phase and explains the weakened Hadley circulation observed during the active phase in the idealized and realistic solar-forced experiments (Fig. 4g, i). A weakening of the Pacific high during the active-period years is also seen in both solar experiments (Fig. 4h, j), which is a crucial factor in the development of the solar SST footprint. In both experiments, the tropical central Pacific Ocean is warmer during active solar periods compared to inactive solar periods (see Supplementary Fig. 11). This warming weakens the Pacific Walker circulation in the experiments, leading to an eastward shift in tropical convection, a decrease in VWS (Supplementary Fig. 13a), and an increase in positive low-level relative vorticity in the central tropical Pacific (Supplementary Fig. 13b). As a result, the results from both the idealized and realistic solar-forced model experiments support our conclusion that the subtropical Pacific SST footprint of the 11-year solar cycle can intrude into the tropical Pacific, creating atmospheric conditions that are favorable (or unfavorable) for typhoon genesis and intensification during its active (or inactive) periods.

**The AMO modulation of the typhoon–solar cycle relationship**
Another major question that needs to be addressed is why the modulation of off-season super typhoon occurrence by the solar cycle intensified after the 1990s. To investigate the potential impact of natural decadal variability, the phase information of the

PDO and AMO is added to Fig. 1c. The results suggest that the solar modulation effect, i.e., the running correlation between SSN and off-season super typhoon number, is more closely related to the AMO phase than the PDO phase. The modulation effect is strong during decades when the AMO is in its positive phase, including the periods before the 1960s and after the 1990s. The correlation coefficient between the running correlation of Fig. 1c and the AMO index is 0.68 ($P < 0.1$), while the correlation with the PDO index is only 0.15 ($P > 0.1$). We replicated the analysis using both a 15-year running correlation and a 27-year running correlation (Supplementary Fig. 14) and find correlation outcomes continue to exhibit a more pronounced connection with the AMO phases as opposed to the PDO phases. Our findings align with prior research indicating a diminished PDO impact on the Pacific climate post-1990s[30], while concurrently observing an augmented influence of AMO on the Pacific climate during the same timeframe[31]. Previous studies[32,33] have also shown that a positive phase of the AMO can enhance the ocean-atmosphere couplings in the subtropical Pacific, which is the central mechanism that gives rise to the solar SST footprint. Therefore, the effect of the solar cycle is magnified during positive AMO decades, explaining why the solar cycle modulation of off-season typhoons has intensified since the AMO switched to a positive phase in the 1990s.

The in-phase correlation found between the solar cycle and off-season typhoons is opposite to that of the out-of-phase correlation reported in previous studies[34–36] between the solar cycle and in-season typhoons. For example, Hung[36] found that the number of in-season typhoons (during the boreal summer and fall) over the western North Pacific decreased (increased) during active (inactive) periods of the solar cycle. Our analysis period (1945–2018) also examines the relationship between solar activity and in-season super typhoon activity and finds a negative correlation ($R = -0.16$ with 0-year lag, $P > 0.1$). The power spectrum of the yearly number of in-season super typhoons reveals a modulation frequency around the 11-year band during the periods 1985–2018 and 1945–2018 (as seen in Supplementary Fig. 15a, b). Apparently, the solar cycle can modulate both in-season and off-season typhoon activities, but in opposite ways. Previous studies[35,36] have presented an in-season modulation mechanism of the solar cycle in which increased solar activity warms the lower stratosphere and upper troposphere during active periods of the solar cycle, reducing the convective available potential energy (CAPE) in the troposphere and preventing hurricane intensification. Our study suggests a similar mechanism for off-season modulation, except that we argue that suppressed convection in the tropics weakens the Hadley circulation, producing a subtropical Pacific SST footprint that intrudes into the tropical Pacific, creating favorable conditions for super typhoon formation. These favorable conditions overcome the unfavorable conditions caused by suppressed tropical convection, leading to an increase in off-season super typhoons during active periods of the solar cycle. The seasonal dependence of the SST footprint mechanism results in opposing relationships between the solar cycle and in-season and off-season typhoon activities. This is because the Hadley circulation is strong in boreal winter but weak in boreal summer[37], meaning the SST footprint mechanism only affects off-season (i.e., boreal winter and spring) typhoons and not in-season typhoons.

## DISCUSSION
The results of our observational analyses and climate model experiments suggest that the 11-year solar cycle can modulate the occurrence of super typhoons over the western North Pacific during the typhoon off-season. The mechanism uncovered in this study not only explains how the modulation effect is produced, but also why it intensified after the 1990s and why it differs from
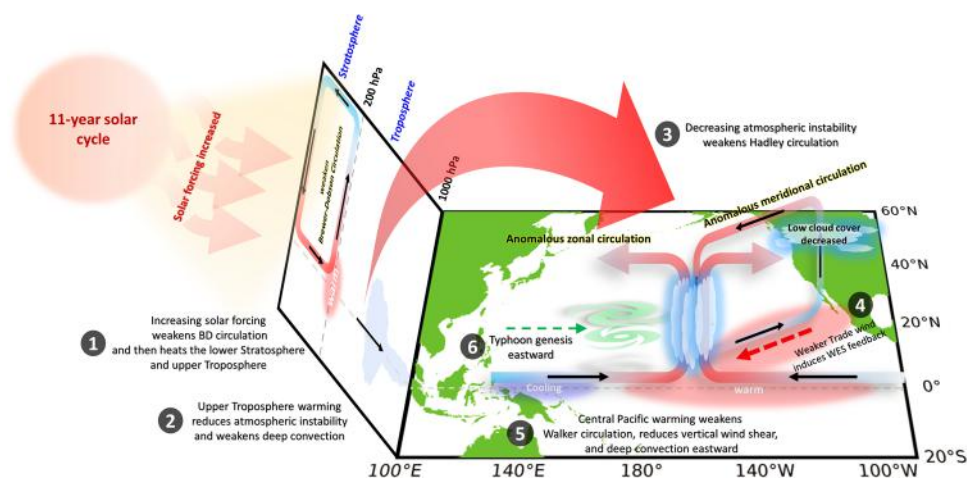
**Fig. 5 Key physical processes linking the 11-year solar cycle to off-season super typhoon activity in the North Pacific.** Taking the solar active period as an example, the following impacts occur: (1) The increased solar forcing increases the latitudinal temperature gradient in the stratosphere, weakening the Brewer-Dobson circulation (BDC) and resulting in anomalous descending motions in the tropics that heat the lower stratosphere and upper troposphere. (2) The upper tropospheric warming reduces tropospheric instability and weakens deep convection in the tropical Pacific, leading to a decrease in in-season (i.e., the May-through-October of the solar cycle year) typhoon activity. (3) The weakened atmospheric instability also weakens the Hadley circulation in the Northern Hemisphere (which typically manifests during the boreal winter of the year). (4) The change in the Hadley circulation strength results in a warm SST anomaly that extends from the Northeastern Pacific into the tropical central Pacific through the wind-evaporation-SST feedback. (5) The resulting warm SSTs eventually arrive in the tropical central Pacific during the following boreal winter and spring seasons (i.e., November of the solar cycle year through the April of the next year) to weaken the Pacific Walker circulation, creating favorable atmospheric conditions for off-season (i.e., November of the solar cycle year through April of the next year) typhoons, including decreased vertical wind shear and increased positive low-level relative vorticity anomalies. (6) The resulting atmospheric conditions cause off-season typhoons to form further eastward than usual, move slower, and spend more time over the ocean, which increases the likelihood of super typhoons forming.

the modulation effect on in-season typhoons reported in previous studies. Figure 5 depicts the sequence of physical processes involved in the modulation mechanism.

For example, stronger radiative forcing during the active period of the solar cycle is first amplified in the stratosphere by the BDC, causing warming in the lower stratosphere and upper troposphere (Step 1). The reduced tropospheric instability leads to a weakening of deep convection in the tropics (Step 2), which directly decreases typhoon activity[36]. This direct impact of the solar cycle is the reason for the negative correlation between the solar cycle and in-season typhoon activity. The reduced atmospheric instability also weakens the Hadley circulation in the Northern Hemisphere (which typically manifests during the boreal winter of the year) (Step 3). This results in a weakened North Pacific subtropical high-pressure system. The resulting weaker trade winds subsequently warm the northeastern Pacific SSTs, and the warm anomalies spread into the tropical central Pacific through the Wind-Evaporation-SST feedback[27,38] (Step 4). Via this solar footprint mechanism, the solar cycle-induced warm SSTs eventually reach the tropical central Pacific during the subsequent boreal winter and spring seasons (i.e., from November of the solar cycle year through April of the following year). This leads to the weakening of the Walker circulation, causing a shift in deep convection eastward and the development of decreased vertical wind shear and positive low-level relative vorticity anomalies (Step 5). These atmospheric conditions then contribute to the development of off-season typhoons (i.e., from November of the solar cycle year through April of the following year) further to the east than usual. These typhoons move at a slower pace and linger over the ocean for extended periods, allowing them more time to absorb moisture from the ocean. This, in turn, increases the likelihood of these typhoons intensifying into super typhoons (Step 6).

This modulation mechanism explains both the in-phase correlation of the solar cycle with off-season typhoon activity and the out-of-phase correlation with in-season typhoon activity. A positive phase of the AMO strengthens Step 3 (and subsequent

steps) of the mechanism, intensifying the solar cycle modulation on off-season super typhoons after the 1990s.

It is important to highlight that our research accentuates the prolonged duration of typhoons resulting from the eastward shift in the favorable atmospheric conditions facilitated by the solar cycle. We have also determined that there is no substantial alteration in the number of typhoons formed during the active and inactive phases of the solar cycle. Consequently, the influence of the solar cycle is predominantly evident in the count of off-season super typhoons, rather than encompassing all off-season typhoon occurrences.

Typhoons that happen during a time other than the normal season (known as off-season typhoons) can cause significant harm to both property and life. The discovery of the decade-long modulation of their occurrence highlights the potential for using information about the solar cycle, such as sunspot numbers, in disaster preparation and management planning at the decadal level.

The conclusions presented in this study rely on a combination of observational analysis and numerical experiments using the NCAR CESM1. Consequently, the outcomes may be influenced by the specific model employed. To address this potential model-dependent variability, it would be beneficial to replicate the experiments with a diverse set of contemporary coupled climate models in the future. Such an investigation can not only help assess model sensitivity of the results but also provide a much larger sample size to further examine the robustness of the findings.

## METHODS

### Observations and reanalysis data
a. The information on typhoon intensity and tracks were obtained from the best track database of the US Joint Typhoon Warning Center (JTWC) since 1945 to 2019.

The PDI[3,22,39] is defined by

$$PDI = \int_0^\varepsilon v_{max}^3 dt \qquad (1)$$

where $v_{max}$ is the maximum surface wind speed at each 6-hourly time interval ($t$) over the typhoon duration ($\varepsilon$). The annual mean typhoon season PDI is the summation of all of the cases (N) in a typhoon season in a year[3,22,39].

The LMI is defined using maximum surface wind speed over the lifetime of a tropical cyclone[19–21]. The typhoon duration was defined using typhoon lifetime, from the point in time when typhoon winds first exceeded 34 knots to time when winds decreased to less than 34 knots.

b. The information on sunspot number (SSN) was obtained from the World Data Center SILSO, Royal Observatory of Belgium, Brussels since 1749 to the present.

c. The monthly values of the TSI were estimated by Kopp et al.[40] using the Community-Consensus TSI Composite and models and obtained from Gregg Kopp's TSI Page, University of Colorado.

d. For sea surface temperatures, the Extended Reconstructed Sea Surface Temperature, version 5 (ERSST v5) data was used. The monthly SSTs from ERSST v5 were provided by the NCEI/NOAA (National Centers for Environmental Information/National Oceanic and Atmospheric Administration) with 2° horizontal resolution from 1854 to the present. The linear trends were removed.

e. The three sets of wind speed and sea level pressure data used in this study were the ECMWF Reanalysis v5 (ERA5) (https://www.ecmwf.int/en/forecasts/datasets/reanalysis-datasets/era5), the Japanese 55-year Reanalysis (JRA55) (https://climatedataguide.ucar.edu/climate-data/jra-55), and the National Centers for Environmental Prediction/National Center for Atmospheric Research (NCEP/NCAR) (https://psl.noaa.gov/data/gridded/data.ncep.reanalysis.html) reanalysis[41]. The monthly ERA5 products were provided on a global 0.25° horizontal grid and 37 vertical levels for the years 1950 to the present. The monthly JRA55 products were provided on a global 1.25° horizontal grid and 37 vertical levels for the years 1957 to the present. The monthly NCEPr1 products were provided on a global 1.875° horizontal grid and 17 vertical levels for the years 1948 to the present. Linear trends in each dataset were removed.

Vertical wind shear (see Eq. 2)[42], and relative vorticity were derived from zonal and meridional wind velocities using the following formulas:

$$vertical\ wind\ shear (VWS) = \sqrt{(U_{200} - U_{850})^2 + (V_{200} - V_{850})^2}$$
$$(2)$$

where $U_{200}$ ($V_{200}$) and $U_{850}$ ($V_{850}$) are the zonal and meridional wind components at the 200 and 850 hPa atmospheric levels.

f. The DGPI is defined by[11]

$$DGPI = (2 + 0.1 \times VWS)^{-1} \times (5.5 - U_y \times 10^5)^2 \times (5 - 20 \times w)^3$$
$$\times (5.5 + \zeta_a \times 10^5)^2 \times e^{-12} - 1.0$$

where VWS, $U_y$, $w$, $\zeta_a$ are vertical wind shear, meridional gradient of zonal wind (at 500 hPa), vertical verocity (at 500 hPa) and absolute vorticity (at 850 hPa), respectively.

g. The D26 were obtained from the NCEP Global Ocean Data Assimilation System (GODAS). The GODAS data provided by the NOAA/OAR/ESRL PSL, Boulder, CO, USA, via their Web site at a 0.333° × 1° horizontal resolution and at 40 vertical levels for the years 1980 to the present. The linear trends were removed.

**Idealized CESM1 solar forcing experiments**

A pair of model experiments were conducted using the CEMS1.2.2 (refer to https://www.cesm.ucar.edu/models/cesm1.2/ for more details). Both the control and solar experiments were conducted using the B1850C5CN (fully coupled)

compset of the CESM1.2.2 with the f19_g16 model configuration, which has a horizontal resolution of approximately 2° and a vertical resolution of 30 vertical levels in the Community Atmospheric Model version 5.3 (CAM5.3) and a horizontal resolution of approximately 1° and 60 vertical levels for the Parallel Ocean Program version 2 (POP2). The total solar irradiation (TSI) is fixed at a constant value (1361 W/m²) in the control experiment but varies in the solar experiment according to the solar cycle variations observed during AD850–959 multiplied by five (i.e., the red line in Supplementary Fig. 9a). The observed TSI variations during this period (i.e., the black line in Supplementary Fig. 9a) is obtained from the CESM dataset (i.e., /glade/p/cesmdata/cseg/inputdata/atm/cam/solar/SOLAR_SPEC-TRAL_VK_Lean_849-2008_annual_c130909.nc), which is constructed by combining the Vieira, Solanki, Krivova, and Usoskin[43] TSI reconstruction and the 11-year solar cycle information from Schmidt et al.[44]. Both experiments were integrated for 110 years from AD850 to 959. All other forcings during the integration period are identical for the both experiments and are provided by the CESM's 850AD-1849 Last Millennium setup, which includes volcanic forcing, greenhouse gas forcing, land use/land cover boundary condition conditions, orbital forcing, aerosol forcing, and ozone forcing.

**The solar forcing-only historical simulation with the GISS-E2-2-G model**

A solar forcing-only historical simulation (commonly referred to as the "hist-sol simulation") produced by the GISS-E2-2-G was used in this study to examine the impacts of the solar forcing on large-scale atmospheric and oceanic variables. The hist-sol simulation was produced by NASA Goddard Institute for Space Studies. A detailed description of this model is available at https://data.giss.nasa.gov/modelE/cmip6/ datalicense. Gillett et al.[45] describe the detailed setup of the solar forcing-only historical simulation. The GISS-E2-2-G model is a high-top model and has a horizontal resolution of approximately 2° × 2.5° and 102 vertical levels (top at the level 0.002 hPa) in the atmosphere, and a horizontal resolution of approximately 1° with 40 vertical levels in the ocean. The hist-sol experiments were integrated for 165 years with the solar forcing observed from 1850 to 2014. The observed TSI variations during this period (i.e., Supplementary Fig. 9b) were obtained from the CMIP dataset (https://solarisheppa.geomar.de/cmip6)[46]. All other external forcings were held at preindustrial values in the hist-sol simulation, including the greenhouse gas concentrations.

*Climate indices.* The PMM index. Following Chiang and Vimont[28], the PMM index is defined as the SST anomalies (i.e., deviations from the monthly climatology) averaged over the PMM region in the North Pacific (10–20°N and 160–120°W) during November-to-April (the typhoon off-season).

*The AMO index.* The values of AMO index are obtained from the NOAA. This index is defined as the detrended SST anomalies averaged over the North Atlantic from the equator to the 70°N[47].

*The PDO index.* The values of this index are also obtained from the NOAA. This index is defined as the principal component of the first EOF mode of the North Pacific SST anomalies[48].

*$SSN_{max}$ and $SSN_{min}$ periods of the solar cycle.* To contrast the large-scale environments between active and inactive periods of the solar cycle in Fig. 3, we define periods with SSN ≥ 100 to be the $SSN_{max}$ (i.e., active) periods and periods with SSN ≤ 20 to be the $SSN_{min}$ (i.e., inactive)[49]. As an example of this selection procedure, the $SSN_{max}$ periods selected during the analysis period are shaded pink in Fig. 1b.

*Significance tests.* We determine the statistical significance levels using the two-tailed *P* values from a Student's *t* test. The effective number of degrees of freedom is determined by considering the auto-correlation of the tested variables.

## DATA AVAILABILITY

Data on typhoon intensity and tracks were acquired from the JTWC's best track database, which can be accessed at https://www.metoc.navy.mil/jtwc/jtwc.html. Information on SSN was obtained from the World Data Center SILSO's datafiles, available at http://www.sidc.be/silso/datafiles. The TSI monthly values were obtained from the TSI Page at the University of Colorado maintained by Gregg Kopp, which can be accessed at https://spot.colorado.edu/~koppg/TSI/. Monthly SSTs were provided by NCEI/NOAA's ERSST v5, which can be accessed at https://www.ncdc.noaa.gov/data-access/marineocean-data/extended-reconstructed-sea-surface-temperature-ersst-v5. Wind speed and sea level pressure data from ERA5, JRA55, and NCEPr1 were obtained from https://www.ecmwf.int/en/forecasts/datasets/reanalysis-datasets/era5, https://climatedataguide.ucar.edu/climate-data/jra-55, and https://psl.noaa.gov/data/gridded/data.ncep.reanalysis.html, respectively. The GODAS data was provided by NOAA/OAR/ESRL PSL in Boulder, Colorado, USA through their website at https://psl.noaa.gov/data/gridded/data.godas.html. The hist-sol simulation was accessed at https://esgf-node.llnl.gov/search/cmip6/. The values of the AMO and PDO indices were obtained from the NOAA website at https://psl.noaa.gov/data/timeseries/AMO/ and https://psl.noaa.gov/pdo/. The idealized CESM1 solar forcing simulations data used in this study can be obtained by contacting Y.-F.L. at yongfulin0711@gmail.com.

## CODE AVAILABILITY

Relevant codes required to replicate the results presented in this study can be obtained from the authors upon request.

## REFERENCES

1. Mori, N. et al. Local amplification of storm surge by Super Typhoon Haiyan in Leyte Gulf. *Geophys. Res. Lett.* **41**, 5106–5113 (2014).
2. Lander, M., Guard, C. & Camargo, S. J. Tropical cyclones, Super Typhoon Haiyan, in state of the climate in 2013. *Bull. Am. Meteor. Soc.* **95**, S112–S114 (2014).
3. Lin, I.-I. & Chan, J. C. L. Recent decrease in typhoon destructive potential and global warming implications. *Nat. Commun.* **6**, 7182 (2015).
4. Braun, H. et al. Possible solar origin of the 1,470-year glacial climate cycle demonstrated in a coupled model. *Nature* **438**, 208–211 (2005).
5. Hathaway, D. H. The solar cycle. *Living Rev. Solar Phys.* **12**, 1 (2015).
6. Palmen, E. On the formation and structure of tropical hurricanes. *Geophysica* **3**, 26–38 (1948).
7. Shay, L. K., Goni, G. J. & Black, P. G. Effects of a warm oceanic feature on Hurricane Opal. *Mon. Wea. Rev.* **128**, 1366–1383 (2000).
8. Pun, I.-F., Lin, I.-I., Wu, C.-R., Ko, D.-S. & Liu, W. T. Validation and application of altimetry-derived upper ocean thermal structure in the Western North Pacific Ocean for typhoon-intensity forecast. *IEEE Trans. Geosci. Remote Sens.* **45**, 1616–1630 (2007).
9. Lin, I.-I., Wu, C.-C., Pun, I.-F. & Ko, D.-S. Upper-ocean thermal structure and the Western North Pacific category 5 typhoons. Part I: Ocean features and the category 5 typhoons' intensification. *Mon. Weather Rev.* **136**, 3288–3306 (2008).
10. Goni, G. et al. Applications of satellite-derived ocean measurements to tropical cyclone intensity forecasting. *Oceanography* **22**, 190–197 (2009).
11. Wang, B. & Murakami, H. Dynamic genesis potential index for diagnosing present-day and future global tropical cyclone genesis. *Environ. Res. Lett.* **15**, 114008 (2020).
12. Lindzen, R. S. & Nigam, S. On the role of sea surface temperature gradients in forcing low-level winds and convergence in the tropics. *J. Atmos. Sci.* **44**, 2418–2436 (1987).
13. Briegel, L. M. & Frank, W. M. Large-scale influences on tropical cyclogenesis in the Western North Pacific. *Mon. Weather Rev.* **125**, 1397–1413 (1997).
14. Simpson, J., Ritchie, E., Holland, G. J., Halverson, J. & Stewart, S. Mesoscale interactions in tropical cyclone genesis. *Mon. Weather Rev.* **125**, 2643–2661 (1997).
15. Chan, J. C. L. & Liu, K. S. Global warming and Western North Pacific typhoon activity from an observational perspective. *J. Clim.* **17**, 4590–4602 (2004).
16. Chen, S. S., Knaff, J. A. & Marks, F. D. Effects of vertical wind shear and storm motion on tropical cyclone rainfall asymmetries deduced from TRMM. *Mon. Weather Rev.* **134**, 3190–3208 (2006).
17. Wang, B. & Chan, J. C. How strong ENSO events affect tropical storm activity over the western North Pacific. *J. clim.* **15**, 1643–1658 (2002).
18. Zheng, Z. W., Lin, I. I., Wang, B., Huang, H. C. & Chen, C. H. A long neglected damper in the El Niño—typhoon relationship: a 'Gaia-like'process. *Sci. Rep.* **5**, 11103 (2015).
19. Emanuel, K. A. A statistical analysis of tropical cyclone intensity. *Mon. Weather Rev.* **128**, 1139–1152 (2000).
20. Kossin, J. P., Emanuel, K. A. & Vecchi, G. A. The poleward migration of the location of tropical cyclone maximum intensity. *Nature* **509**, 349–352 (2014).
21. Lee, C.-Y., Tippett, M. K., Sobel, A. H. & Camargo, S. J. Rapid intensification and the bimodal distribution of tropical cyclone intensity. *Nat. Commun.* **7**, 1–5 (2016).
22. Emanuel, K. Increasing destructiveness of tropical cyclones over the past 30 years. *Nature* **436**, 686–688 (2005).
23. Lin, Y.-F., Yu, J.-Y., Wu, C.-R. & Zheng, F. The footprint of the 11-year solar cycle in Northeastern Pacific SSTs and its influence on the Central Pacific El Niño. *Geophys. Res. Lett.* **48**, e2020GL091369 (2021).
24. Huo, W., Xiao, Z., Wang, X. & Zhao, L. Lagged responses of the tropical Pacific to the 11-yr solar cycle forcing and possible mechanisms. *J. Meteor. Res.* **35**, 444–459 (2021).
25. Kodera, K. & Kuroda, Y. Dynamical response to the solar cycle. *J. Geophys. Res. Atmos.* **107**, ACL 5-1–ACL 5-12 (2002).
26. Yu, J.-Y. & Fang, S.-W. The distinct contributions of the seasonal footprinting and charged-discharged mechanisms to ENSO complexity. *Geophys. Res. Lett.* **45**, 6611–6618 (2018).
27. Xie, S.-P. & Philander, S. G. H. A coupled ocean-atmosphere model of relevance to the ITCZ in the eastern Pacific. *Tellus A Dyn. Meteorol. Oceanogr.* **46**, 340–350 (1994).
28. Chiang, J. C. H. & Vimont, D. J. Analogous Pacific and Atlantic meridional modes of tropical atmosphere-ocean variability. *J. Clim.* **17**, 4143–4158 (2004).
29. Yu, J.-Y., Wang, X., Yang, S., Paek, H. & Chen, M. in *Climate Extremes: Patterns and Mechanisms* 1–38 (Wiley, 2017).
30. Wu, C.-R., Wang, Y.-L. & Chao, S.-Y. Disassociation of the Kuroshio current with the Pacific decadal oscillation since 1999. *Remote Sens.* **11**, 276 (2019).
31. Wang, L., Yu, J.-Y. & Paek, H. Enhanced biennial variability in the Pacific due to Atlantic capacitor effect. *Nat. commun.* **8**, 14887 (2017).
32. Yu, J.-Y. et al. Linking emergence of the Central Pacific El Niño to the Atlantic multidecadal oscillation. *J. Clim.* **28**, 651–662 (2015).
33. Lyu, K., Yu, J.-Y. & Paek, H. The influences of the Atlantic Multidecadal Oscillation on the mean strength of the North Pacific subtropical high during boreal winter. *J. Clim.* **30**, 411–426 (2017).
34. Cohen, T. J. & Sweetser, E. I. The 'spectra' of the solar cycle and of data for Atlantic tropical cyclones. *Nature* **256**, 295–296 (1975).
35. Elsner, J. B. & Jagger, T. H. United States and Caribbean tropical cyclone activity related to the solar cycle. *Geophys. Res. Lett.* **35**, L18705 (2008).
36. Hung, C.-W. A 300-year typhoon record in Taiwan and the relationship with solar activity. *Atmos. Ocean Sci.* **24**, 737 (2013).
37. Lindzen, R. S. & Hou, A. V. Hadley circulations for zonally averaged heating centered off the equator. *J. Atmos. Sci.* **45**, 2416–2427 (1988).
38. Wang et al. Evaluation of performance of CMIP5 models in simulating the North Pacific Oscillation and El Niño Modoki. *Clim. Dyn.* **52**, 1383–1394 (2019).
39. Emanuel, K. Environmental factors affecting tropical cyclone power dissipation. *J. Clim.* **20**, 5497–5509 (2007).
40. Kopp, G., Krivova, N., Wu, C. J. & Lean, J. The impact of the revised sunspot record on solar irradiance reconstructions. *Sol. Phys.* **291**, 2951–2965 (2016).
41. Kalnay, E. et al. The NCEP/NCAR 40-year reanalysis project. *Bull. Am. Meteorol. Soc.* **77**, 437–471 (1996).
42. Huang, H.-C. et al. Air-sea fluxes for Hurricane Patricia (2015): comparison with supertyphoon Haiyan (2013) and under different ENSO conditions. *J. Geophys. Res. Oceans* **122**, 6076–6089 (2017).
43. Vieira, L. E. A., Solanki, S. K., Krivova, N. A. & Usoskin, I. Evolution of the solar irradiance during the Holocene. *Astron. Astrophys.* **531**, A6 (2011).
44. Schmidt, G. A. et al. Climate forcing reconstructions for use in PMIP simulations of the Last Millennium (v1.1). *Geosci. Model Dev.* **5**, 185–191 (2012).
45. Gillett, N. P. et al. The detection and attribution model intercomparison project (DAMIP v1. 0) contribution to CMIP6. *Geosci. Model Dev.* **9**, 3685–3697 (2016).
46. Matthes, K. et al. Solar forcing for CMIP6 (v3. 2). *Geosci. Model Dev.* **10**, 2247–2302 (2017).
47. Enfield, D. B., Mestas-Nuñez, A. M. & Trimble, P. J. The Atlantic multidecadal oscillation and its relation to rainfall and river flows in the continental U.S. *Geophys. Res. Lett.* **28**, 2077–2080 (2001).
48. Mantua, N. J., Hare, S. R., Zhang, Y., Wallace, J. M. & Francis, R. C. A Pacific interdecadal climate oscillation with impacts on salmon production. *Bull. Am. Meteorol. Soc.* **78**, 1069–1079 (1997).

49. Ratnam, V. M., Rao, V. N., Vedavathi, C., Murthy, K. B. V. & Bhaskara Rao, V. S. Diurnal tide in the low-latitude troposphere and stratosphere: long-term trends and role of the extended solar minimum. *J. Atmos. Sol. Terr. Phys.* **121**, 168–176 (2014).

## ACKNOWLEDGEMENTS

## AUTHOR CONTRIBUTIONS

C.-R.W., Y.-F.L., and J.-Y.Y. developed the initial concept for the study and drafted the paper. J.-Y.Y. and Y.-F.L. designed the model experiments and analyses. Y.-F.L. was responsible for executing the simulations and analyzing the data. I.-I.L. collaborated in the interpretation of the results.

## COMPETING INTERESTS

The authors declare no competing interests.

## ADDITIONAL INFORMATION

**Supplementary information** The online version contains supplementary material available at https://doi.org/10.1038/s41612-023-00495-z.

**Correspondence** and requests for materials should be addressed to Chau-Ron Wu or Jin-Yi Yu.

**Reprints and permission information** is available at http://www.nature.com/reprints

**Publisher's note** Springer Nature remains neutral with regard to jurisdictional claims in published maps and institutional affiliations.